A Novel Small-Molecule Inhibitor of Protein Kinase Cι Blocks Transformed Growth of Non–Small-Cell Lung Cancer Cells

Melody Stallings-Mann, Lee Jamieson, Roderick P. Regala, Capella Weems, Nicole R. Murray, and Alan P. Fields

Department of Cancer Biology, Mayo Clinic College of Medicine, Jacksonville, Florida

Abstract

We recently showed that atypical protein kinase Cι (PKCι) is required for transformed growth of human non–small-cell lung cancer (NSCLC) cells by activating Rac1. Genetic disruption of PKCι signaling blocks Rac1 activity and transformed growth, indicating that PKCι is a viable target for development of novel therapeutics for NSCLC. Here, we designed and implemented a novel fluorescence resonance energy transfer–based assay to identify inhibitors of oncogenic PKCι signaling. This assay was used to identify compounds that disrupt the interaction between PKCι and its downstream effector Par6, which links PKCι to Rac1. We identified aurothioglucose (ATG), a gold compound used clinically to treat rheumatoid arthritis, and the related compound, aurothiomalate (ATM), as potent inhibitors of PKCι-Par6 interactions *in vitro* (IC_{50} ~1 μmol/L). ATG blocks PKCι-dependent signaling to Rac1 and inhibits transformed growth of NSCLC cells. ATG-mediated inhibition of transformation is relieved by expression of constitutively active Rac1, consistent with a mechanism at the level of the interaction between PKCι and Par6. ATG inhibits A549 cell tumor growth in nude mice, showing efficacy against NSCLC in a relevant preclinical model. Our data show the utility of targeting protein-protein interactions involving PKCι for antitumor drug development and provide proof of concept that chemical disruption of PKCι signaling can be an effective treatment for NSCLC. ATG and ATM will be useful reagents for studying PKCι function in transformation and represent promising new agents for the clinical treatment of NSCLC. (Cancer Res 2006; 66(3): 1767-74)

Introduction

Lung cancer is the leading cause of cancer death in the United States, accounting for an estimated 160,440 deaths in 2004 (1). Most lung cancers (~80%) are classified as non–small-cell lung cancer (NSCLC), with most remaining cases (~18%) being small-cell lung cancer (2). Early-stage NSCLC tumors are often treated with surgery and radiotherapy whereas advanced-stage metastatic disease often receives combination chemotherapy (2). Unfortunately, despite surgical removal and adjuvant therapy, many early-stage NSCLCs relapse and become fatal. The 5-year survival rate for NSCLC is only 14%, underscoring the need for more effective modalities for prognosis, prevention, and treatment.

Recently, we showed that the atypical protein kinase C (PKC) isozyme, PKCι, plays a requisite role in NSCLC cell growth (3). Expression of PKCι is elevated in established human NSCLC cell lines and genetic disruption of PKCι signaling by expression of a dominant-negative, kinase-deficient PKCι allele blocks anchorage-independent transformed growth and tumorigenicity of NSCLC cells in nude mice (3). PKCι expression is also elevated in the vast majority of primary NSCLC tumors and PKCι expression correlates with poor survival in patients with NSCLC (4). PKCι expression predicts poor survival independent of tumor stage, indicating that PKCι expression may be useful in identifying NSCLC patients with early-stage disease who are at elevated risk for relapse. In addition, the PKCι gene is a frequent target for tumor-specific gene amplification in a significant subset of NSCLC, particularly in squamous cell carcinoma of the lung (4). PKCι gene amplification drives PKCι expression and disruption of PKCι signaling in NSCLC cells that harbor PKCι gene amplification blocks transformed growth, showing the importance of PKCι gene amplification in NSCLC biology (4). Taken together, our data identified PKCι as a critical oncogene in NSCLC.

A major molecular mechanism by which PKCι drives transformed growth was recently elucidated by our laboratory. Specifically, we showed that PKCι is required for NSCLC transformation by activating a PKCι→Rac1→Pak→Mek→Erk signaling axis that is required for transformed growth *in vitro* and *in vivo* (3). Furthermore, we showed that expression of the PB1 domain within the NH_2-terminal regulatory region of PKCι blocks transformed growth by uncoupling PKCι from Rac1 activation (3). Taken together, our data suggest that PKCι is an attractive target for the development of mechanism-based therapeutics for the treatment of NSCLC. Here, we report the design and use of a novel fluorescence resonance energy transfer (FRET)–based high-throughput assay to identify chemical inhibitors of the interaction between PKCι and its effector Par6. Using this assay, several high-affinity compounds have been identified that disrupt the PB1 domain–mediated interactions between PKCι and Par6. These compounds effectively inhibit PKCι signaling to Rac1, the downstream target of the PKCι-Par6 interaction, and exhibit potent antitumor effects on NSCLC cell growth *in vitro* and *in vivo*. Our data provide important proof of principle that chemical disruption of protein/protein interactions involving the PB1 domain of PKCι is an effective route to the development of novel therapeutics for the treatment of patients with NSCLC.

Materials and Methods

Reagents. The Rac1 antibody was from Transduction Labs (Palo Alto, CA) and was used at a concentration of 1:3,000. Aurothioglucose (ATG) was from Research Diagnostics (Concord, MA). Aurothiomalate (ATM) was from Taylor Pharmaceuticals (Decatur, IL) (Myochrysine). Rac/cdc42 assay reagents were

Note: M. Stallings-Mann and L. Jamieson contributed equally to this work.
Requests for reprints: Alan P. Fields, Department of Cancer Biology, Mayo Clinic Comprehensive Cancer Center, Room 312, Griffin Cancer Research Building, 4500 San Pablo Road, Jacksonville, FL 32224. Phone: 904-953-6160; Fax: 904-953-0277; E-mail: fields.alan@mayo.edu.

doi:10.1158/0008-5472.CAN-05-3405

from Upstate (Charlottesville, VA). The GenPlus Collection of compounds was from Microsource Discovery Systems, Inc. (Gaylordsville, CT).

Plasmids, cloning, and recombinant proteins. The PB1 domain of human PKCι (amino acids 1-113) was generated by PCR amplification of a plasmid containing the full-length human PKCι cDNA (5). The PB1 domain of human Par6 (amino acids 1-125) was generated by PCR amplification from a human K562 cell cDNA library (Clontech, Palo Alto, CA). The PB1 domains of PKCι and Par6 were cloned into the pCR2.1-TOPO transfer vector and subsequently into the pEYFP-N1 and pECFP-N1 eukaryotic expression vectors (BD Biosciences, Palo Alto, CA) to generate pPKCι/YFP and pPar6/CFP, respectively. The pEYFP-N1 and pECFP-N1 vectors were subjected to site-directed mutagenesis to mutate alanine 206 of yellow fluorescent protein (YFP) and cyan fluorescent protein (CFP) to lysine. This amino acid change prevents YFP and CFP from dimerizing, thereby eliminating a potential source for background in FRET-based assays (6, 7). Appropriate primers were used to amplify PKCι/YFP, Par6/CFP, YFP, and CFP and directionally clone them into the pRSET vectors for high-level expression of NH_2-terminally His-tagged fusion proteins in bacteria (Invitrogen, Carlsbad, CA). Isolated clones were transformed into BL21(DE3)pLysS or BL21AI strain of *E. coli* (Invitrogen) for expression and purification. The full-length human Par6α cDNA was generated by PCR from a human K562 cell cDNA library (Clontech) and cloned into the PinPoint Xa-3 vector (Promega, Madison, WI), which allows high-level expression of biotinylated Par6 fusion protein in bacteria. The PB1 domain of PKCι, amplified by PCR as described above, was also cloned into the pGEX-6P-2 vector (Amersham Biosciences, Piscataway, NJ), which allows high-level expression of glutathione *S*-transferase (GST)–tagged PKCι PB1 domain. Isolated clones were transformed into BL21(DE3)pLysS *E. coli* for protein expression and purification. All constructs were verified by sequencing.

Expression, purification, and characterization of recombinant proteins. His-tagged PKCι/YFP, CFP, and YFP recombinant proteins were isolated from the soluble fraction of bacterial lysates by affinity purification using the B-PER 6×His Purification Kit (Pierce, Rockford, IL) and purified proteins were dialyzed against Tris buffer [50 mmol/L Tris (pH 8.0), 135 mmol/L NaCl, 10% glycerol, 0.002% EDTA] containing 2 mol/L urea. His-tagged Par6/CFP recombinant protein was isolated from inclusion bodies using the B-PER reagent (Pierce). Briefly, inclusion bodies were solubilized in Tris buffer containing 8 mol/L urea and dialyzed against the same buffer containing 4 mol/L urea for 4 hours, and then overnight against Tris buffer containing 2 mol/L urea. Yields were quantified by protein assay and measurement of fluorescence in a SpectraMax Gemini microplate reader (Molecular Devices, Union City, CA). Purified recombinant PKCι/YFP, Par6/CFP, YFP, and CFP were analyzed for their spectral properties using a SpectraMax Gemini fluorescence plate reader. Excitation profiles were determined by monitoring emission at 475 nm for CFP and Par6/CFP and at 529 nm for YFP and PKCι/YFP. Emission profiles were obtained using an excitation wavelength of 434 nm for CFP and Par6/CFP and 495 nm for YFP and PKCι/YFP. Results were expressed as normalized fluorescence for each protein.

A FRET-based Par6-PKCι interaction assay and compound library screen. For compound library screening, 50 μL of PKCι/YFP (containing 4,000 fluorescence units) and 50 μL of Par6/CFP (containing 400 fluorescence units) were added to each well of 96-well, clear-bottom black plates (Costar 3631), followed by 10 μL of each of 960 compounds from the MicroSource GenPlus library to a final concentration of 1 mmol/L. Plates were incubated at 4°C for 4 hours and fluorescence emission was measured at 475 nm (cutoff, 455 nm) and 529 nm (cutoff, 515 nm) on a SpectraMax Gemini plate reader using an excitation wavelength of 395 nm. The entire library of compounds was screened in triplicate. Specific FRET was determined by taking the fluorescence ratio (529/475 nm) after subtracting the background ratio in samples using a nonbinding protein pair (Par6/CFP and YFP).

A PKCι-Par6 binding assay. Purified recombinant biotinylated human Par6 [100 μL of a 5 μg/mL solution in PBS containing 0.1% Tween 20 (PBS-Tween 20)] was pipetted into each well of streptavidin-coated 96-well microtiter plates (Nunc, Roskilde, Denmark) and allowed to bind for 2 hours at room temperature. Plates were washed twice with PBS-Tween 20, then once with incubation buffer [50 mmol/L Tris (pH 8.0), 135 mmol/L NaCl, 10% glycerol, 0.002% EDTA, 1 mol/L urea]. After washing, 50 μL of incubation buffer were added to each well followed by 10 μL of either ATG or ATM to a final concentration indicated in the figure legend. PKCι/YFP (4,000 fluorescence units in 40 μL) was added to each well and plates were incubated overnight at 4°C. Plates were washed thrice with PBS and the amount of bound PKCι/YFP fluorescence was determined using a Typhoon 9410 imager (GE Healthcare, Piscataway, NJ). Fluorescence was quantitated using ImageQuant software (Amersham).

Cell culture and transfections. Human A549 NSCLC cells were maintained as previously described (3). A549 cells were stably transfected with recombinant pBabe retroviruses containing Flag-tagged full-length human kinase-deficient PKCι mutant (kdPKCι) or empty pBabe vector as previously described (8). In some experiments, A549 cells were stably transfected with a recombinant LZRS retrovirus containing a full-length human constitutively active Rac1 mutant (RacV12) or empty vector to generate A549/LZRS and A549/RacV12 cells as previously described (9). The adherent growth of A549 cells was determined in the presence and absence of 10 μmol/L ATG by plating cells (1×10^4 per well) into multiwell culture dishes and determining cell number after 4 days using a hemocytometer.

Rac1 activity assay. Rac1 activity was assessed in parental A549 cells in the presence and absence of ATG and in A549/pBabe and A549/kdPKCι cell transfectants as previously described (3, 9). Briefly, cells were lysed in lysis buffer [50 mmol/L Tris-HCl (pH 7.5), 150 mmol/L NaCl, 20 mmol/L $MgCl_2$, 5 mmol/L EGTA, 10% glycerol, 1% Triton X-100, 1% NP40, 25 mmol/L NaF, 1 mmol/L phenylmethylsulfonyl fluoride, 1 mmol/L sodium orthovanadate, 10 μg/mL leupeptin, 10 μg/mL aprotinin] at 4°C for 5 minutes. Cellular debris was removed by centrifugation at 20,000 × *g* for 5 minutes and supernatants were transferred to new tubes. An aliquot of each supernatant was reserved to determine total Rac1 expression by immunoblot analysis before addition of 20 μL of GST-p21-binding domain of PAK1 coupled to agarose beads (Upstate). Following a 30-minute incubation at 4°C, the agarose beads were collected by centrifugation and washed thrice with lysis buffer. Bound proteins were solubilized by the addition of 30 μL of SDS sample buffer, resolved by SDS-PAGE, and subjected to immunoblot analysis for Rac1 as previously described (3, 9). An equivalent amount of cell lysate was subjected to immunoblot analysis to assess total Rac1 expression. Signal intensity was quantitated using ImageQuant software.

Soft agar growth and tumorigenicity assays. Anchorage-independent growth of A549/LZRS and A549/RacV12 cells was assessed by their ability to grow as colonies in soft agar in the presence or absence of 10 μmol/L ATG as previously described (3, 4). The ability of A549 cells to grow as established s.c. tumors and in the presence and absence of ATG was studied in athymic nude mice (Harlan Sprague-Dawley, Indianapolis, IN) as previously described (3). Four- to six-week-old female nude mice were injected s.c. with 5×10^6 A549 cells in 100 μL of growth medium. When tumors had reached an average volume of 50 mm^3 (day 21 postinjection), the mice were randomly divided into two groups. The treatment group received daily injections of ATG at 200 mg/kg and the other group received an equal volume of diluent (0.9% sterile saline) daily for a 2-week period. Tumor dimensions were measured using calipers and tumor volume (mm^3) was calculated using the following formula: 0.5236 ($L \times W \times H$), where L is tumor length, W is width, and H is height. At the conclusion of the study, mice were sacrificed by CO_2 asphyxiation.

Results

A FRET-based assay to detect PB1-PB1 domain interactions between PKCι and Par6. Our previous studies have shown that PKCι is an oncogene in NSCLC (3, 4). Specifically, we showed that PKCι expression is elevated in the majority of NSCLC cell lines and primary tumors, that PKCι expression is predictive of poor outcome in NSCLC patients, and that the PKCι gene is a target for frequent tumor-specific gene amplification in squamous cell carcinoma of the lung (4). Mechanistically, we showed that PKCι activates a PKCι→Rac1→Pak→Mek→Erk pathway that is required for transformed growth *in vitro* and *in vivo* (3). Based on our

studies, we proposed that PKCι is an attractive target for development of novel mechanism-based therapeutics for NSCLC.

To assess the therapeutic potential of PKCι as a drug target, we developed a novel assay using FRET technology to identify potential inhibitors of PKCι signaling. We chose not to screen for compounds that directly inhibit PKCι catalytic activity because the catalytic domain of the enzyme is highly conserved among PKC isozymes and the larger superfamily of protein kinases, making identification of highly specific compounds problematic. Rather, we targeted the PB1 domain of PKCι because it is uniquely present in atypical PKCs and not other PKC isozymes and it is required for the oncogenic function of PKCι (3). The PB1 domain of PKCι represents a highly specific protein-protein interaction domain that mediates binding of PKCι to several adaptor molecules, particularly Par6 and p62, which link PKCι to downstream effector pathways (10). We have shown that expression of the PB1 domain of PKCι blocks PKCι-mediated activation of Rac1 and the transformed growth of A549 lung adenocarcinoma cells (3).

The FRET-based assay was developed to measure binding between the PB1 domains of PKCι and Par6. We chose to use two variants of green fluorescent protein, enhanced CFP and enhanced YFP, because it has been previously shown that these two fluorophores are highly suited for FRET (6, 11, 12). Specifically, the emission spectrum of CFP partially overlaps the excitation spectrum of YFP; both CFP and YFP are relatively photostable; and CFP is sufficiently bright to permit accurate ratiometric measurement of both donor (CFP) and acceptor (YFP) by a variety of fluorescence detectors, including fluorescence plate readers (12). Therefore, we constructed plasmids that allowed us to express and purify the PB1 domain of Par6 as a His-tagged fusion protein with CFP (Par6/CFP) and the PB1 domain of PKCι as a His-tagged fusion protein with YFP (PKCι/YFP; Fig. 1*A*). To determine whether the Par6/CFP and PKCι/YFP fusion proteins retained spectral properties similar to native CFP and YFP proteins, we analyzed the excitation and emission spectra of these proteins compared with His-tagged CFP and His-tagged YFP expressed in the same bacterial system. Both the excitation (Fig. 1*B* and *C*) and emission (Fig. 1*D* and *E*) spectra of Par6/CFP (Fig. 1*B* and *D*) and PKCι/YFP (Fig. 1*C* and *E*) are virtually identical to those of CFP and YFP, respectively.

We next determined whether these proteins are suitable for FRET-based detection of interactions between the PB1 domains of Par6 and PKCι. The basis for the binding assay is illustrated in Fig. 2*A*. Based on the excitation spectral data in Fig. 1, we chose an excitation wavelength of 395 nm, which is within the excitation range of Par6/CFP, but not of PKCι/YFP. Thus, at this wavelength, Par6/CFP should emit blue light that can be detected at 475 nm whereas PKCι/YFP should emit little or no light. When purified Par6/CFP is exposed to 395-nm light, the characteristic emission spectrum of CFP with a peak emission at 475 nm is observed (Fig. 2*B*). In contrast, when purified PKCι/YFP is exposed to 395-nm light, only a small peak is observed at 529 nm, which is not

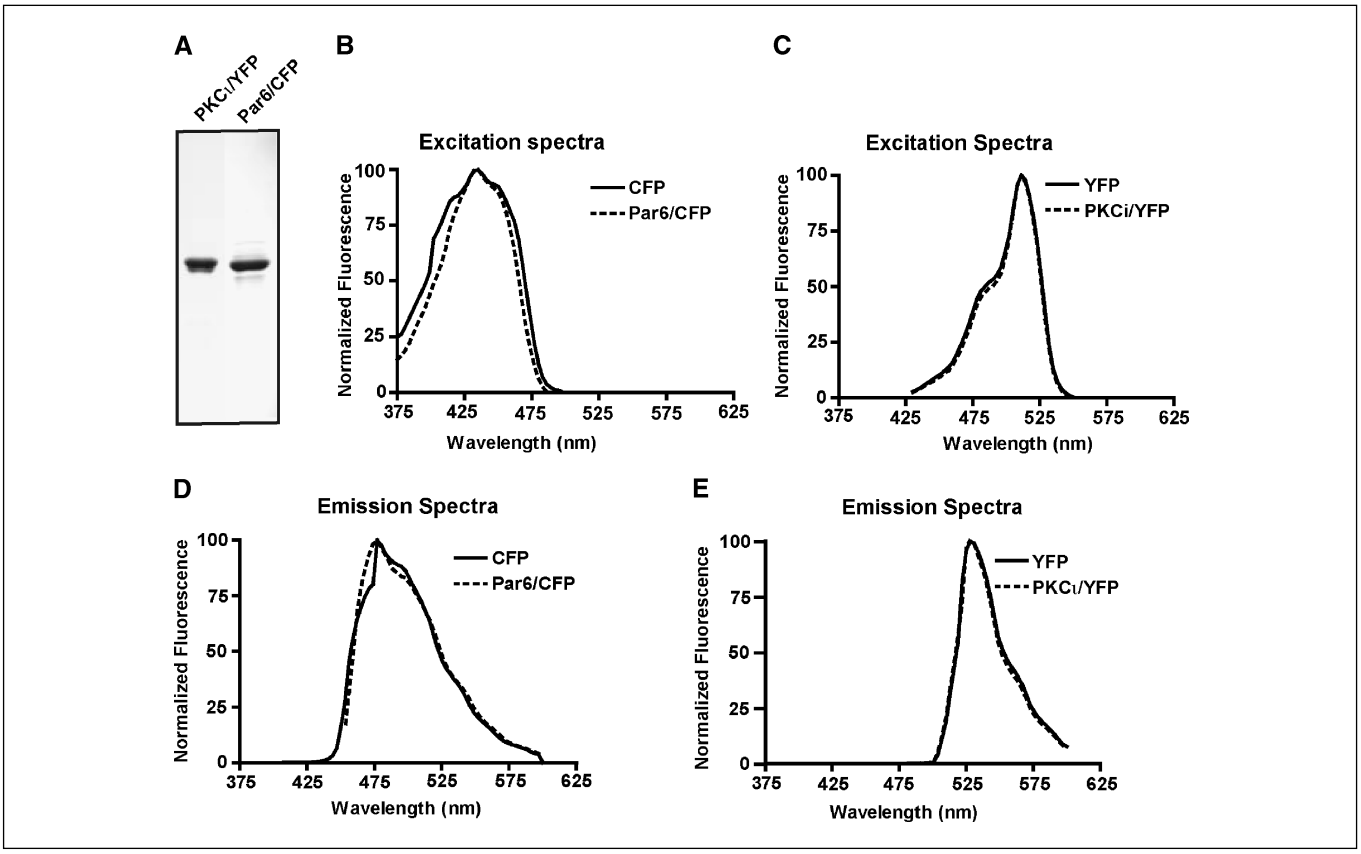

Figure 1. Characterization of Par6/CFP and PKCι/YFP fusion proteins. *A,* Coomassie blue–stained polyacrylamide gel of bacterially expressed and purified PKCι/YFP and Par6/CFP fusion proteins. *B* and *C,* excitation spectra of CFP (*B*) and YFP (*C*; *solid lines*) compared with Par6/CFP (*B*) and PKCι/YFP (*C*; *dashed lines*) fusion proteins, respectively. Emission was measured at 475 nm for CFP and Par6/CFP and at 529 nm for YFP and PKCι/YFP. *D* and *E,* emission spectra of CFP (*D*) and YFP (*E*; *solid lines*) compared with Par6/CFP (*D*) and PKCι/YFP (*E*; *dashed lines*) fusion proteins, respectively. Excitation wavelength was 434 nm for CFP and Par6/CFP and 495 nm for YFP and PKCι/YFP.

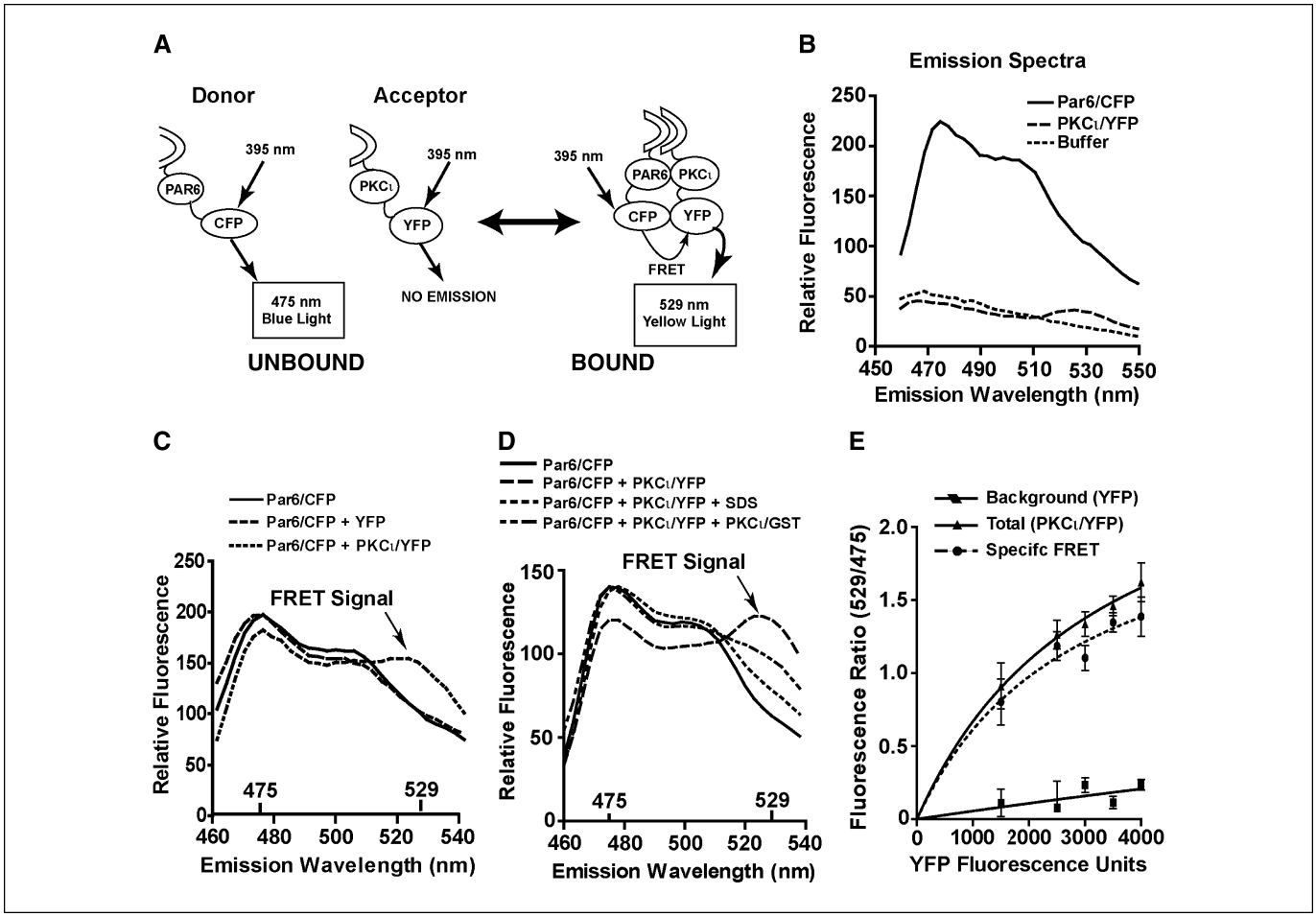

Figure 2. Characterization of a FRET-based assay to measure binding between Par6/CFP and PKCι/YFP. *A,* schematic diagram illustrating the basis of the FRET-based assay for Par6/PKCι interactions. When exposed to 395-nm light, the donor molecule Par6/CFP emits blue fluorescent light with an emission maximum at 475 nm. The acceptor molecule PKCι/YFP does not fluoresce when exposed to 395-nm light. When Par6/CFP and PKCι/YFP bind, excitation of the donor with 395-nm light leads not only to emission of blue light at 475 nm but also to FRET-mediated emission of yellow light at 529 nm. *B,* emission spectra of Par6/CFP and PKCι/YFP fusion proteins alone in solution after exposure to 395-nm light. Par6/CFP emits a spectrum characteristic of CFP whereas PKCι/YFP does not emit appreciably above buffer alone. *C,* emission spectra of the Par6/CFP in the absence of other proteins (*solid line*) when combined with the nonbinding protein partner YFP (*dashed line*) and when combined with its binding partner PKCι/YFP (*dotted line*) after exposure to 395-nm light. *D,* emission spectra of Par6/CFP in the absence (*solid line*) or presence (*long dashed line*) of its binding partner PKCι/YFP. The binding reaction was also carried out in the presence of SDS (*short dashed line*) and a nonfluorescent competitive inhibitor consisting of the PB1 domain of PKCι fused to GST (*dotted line*). *E,* FRET measurements were obtained for Par6/CFP in the presence of increasing amounts of the nonbinding control protein YFP (■) or its binding partner PKCι/YFP (▲). Results are expressed as the fluorescence ratio of emission 529/475 nm. The nonbinding control values were subtracted from the Par6/CFP:PKCι/YFP values to obtain the specific FRET associated with the saturable binding between Par6/CFP and PKCι/YFP (*dotted line*).

appreciably above the background emission associated with buffer alone (Fig. 2*B*). However, when Par6/CFP and PKCι/YFP are incubated together, we observe a decrease in the fluorescence peak at 475 nm associated with Par6/CFP emission and a second emission peak with a maximum at ~529 nm characteristic of FRET (Fig. 2*C*). As expected, no emission peak at 529 nm is observed when Par6/CFP is tested alone or when the nonbinding protein pairs Par6/CFP and YFP are incubated together (Fig. 2*C*). Furthermore, the FRET-mediated emission peak at 529 nm is disrupted by addition of either SDS or an excess of a nonfluorescent fusion protein containing the PB1 domain of PKCι (amino acids 1-113) fused to GST (PKCι/GST; Fig. 2*D*). Taken together, these data show that the fluorescence peak seen at 529 nm is due to FRET produced as a result of binding between Par6/CFP and PKCι/YFP.

Specific FRET between CFP- and YFP-containing binding protein pairs is often expressed as the ratio of the fluorescence emission at 529 and 475 nm (fluorescence ratio 529/475) of a solution containing the CFP/YFP binding pair minus the fluorescence ratio 529/475 of a solution containing equivalent fluorescence units of a nonbinding CFP/YFP pair. To optimize the binding reaction to obtain the highest FRET value with the least interference from direct excitation of unbound PKCι/YFP, we incubated increasing amounts of YFP or PKCι/YFP with a set amount of Par6/CFP (400 fluorescence units; Fig. 2*E*). When increasing amounts of PKCι/YFP are added to a solution of Par6/CFP, the fluorescence ratio 529/475 increases rapidly and exhibits saturable kinetics. In contrast, increasing concentrations of nonbinding YFP cause only a slight increase in the fluorescence ratio 529/475. The specific FRET signal is obtained by subtracting the background fluorescence associated with the nonbinding YFP protein from the fluorescence ratio in the presence of the Par6/CFP and PKCι/YFP binding pairs. This analysis shows that the FRET signal is saturable and defines optimal conditions for measuring the binding of PKCι/YFP and

Par6/CFP by FRET. Thus, these optimized FRET conditions were used to screen our compound library.

Screening of a compound library for inhibitors of PKCι-Par6 interactions. Having developed and optimized a FRET-based assay capable of detecting binding between the PB1 domains of PKCι and Par6, we next screened the GenPlus chemical compound library from Microsource Discovery Systems for compounds that inhibit this binding. The GenPlus library is a unique collection of ~960 known bioactive compounds that permit the simultaneous evaluation of hundreds of marketed drugs and biochemical standards. All of the compounds in the library have well-characterized pharmacokinetic and bioavailability profiles, making them excellent first hit candidates. A representative collection of nine compounds from the library screen are shown in Fig. 3*A*. As can be seen, one of these compounds, ATG, showed a marked decrease in the fluorescence ratio approaching that observed with the control nonbinding protein pair Par6/CFP + YFP (which gave a fluorescence ratio value of ~0.2). Subsequent analysis showed that ATG causes a dose-dependent loss of FRET with maximum inhibition in the 100 μmol/L range with an apparent IC_{50} in the low micromolar range (Fig. 3*B*). Incubation of purified YFP-PKCι or CFP-Par6 alone with ATG at concentrations up to 1 mmol/L had no effect on the intrinsic fluorescence of these proteins, indicating that ATG does not inhibit FRET by quenching CFP or YFP fluorescence (data not shown).

We next wished to confirm that ATG inhibits binding between Par6 and PKCι. For this purpose, we devised a complimentary binding assay. In this assay, full-length biotinylated Par6 was bound to streptavidin-coated 96-well plates and binding of PKCι/YFP was

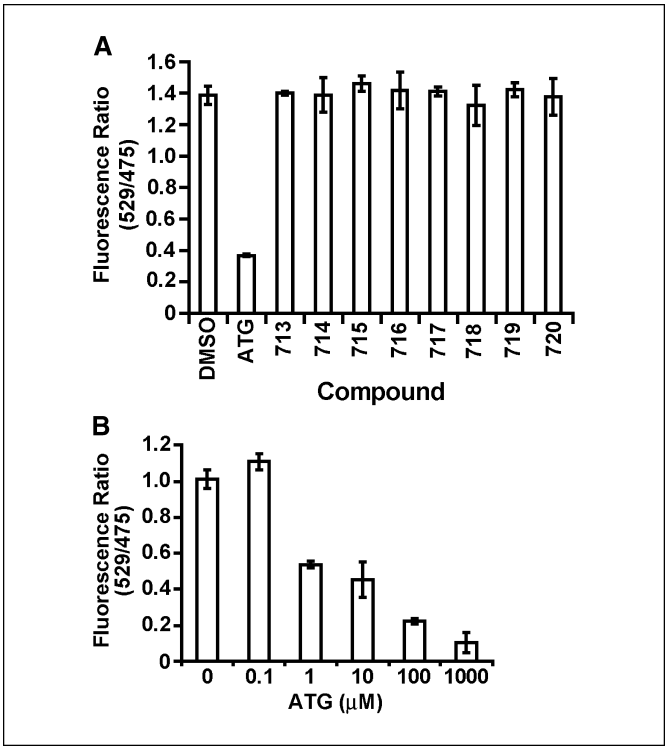

Figure 3. Identification of ATG as an inhibitor of Par6/CFP and PKCι/YFP binding. *A,* ATG disrupts binding between PKCι/YFP and Par6/CFP as shown by loss of FRET. Other representative compounds (713-720) from the library show no inhibitory activity. DMSO is included as a vehicle control. *B,* ATG inhibits binding between Par6/CFP and PKCι/YFP in a dose-dependent fashion. *Columns,* mean fluorescence ratio (529/475 nm) in the presence of the indicated compound (n = 3); *bars,* SE.

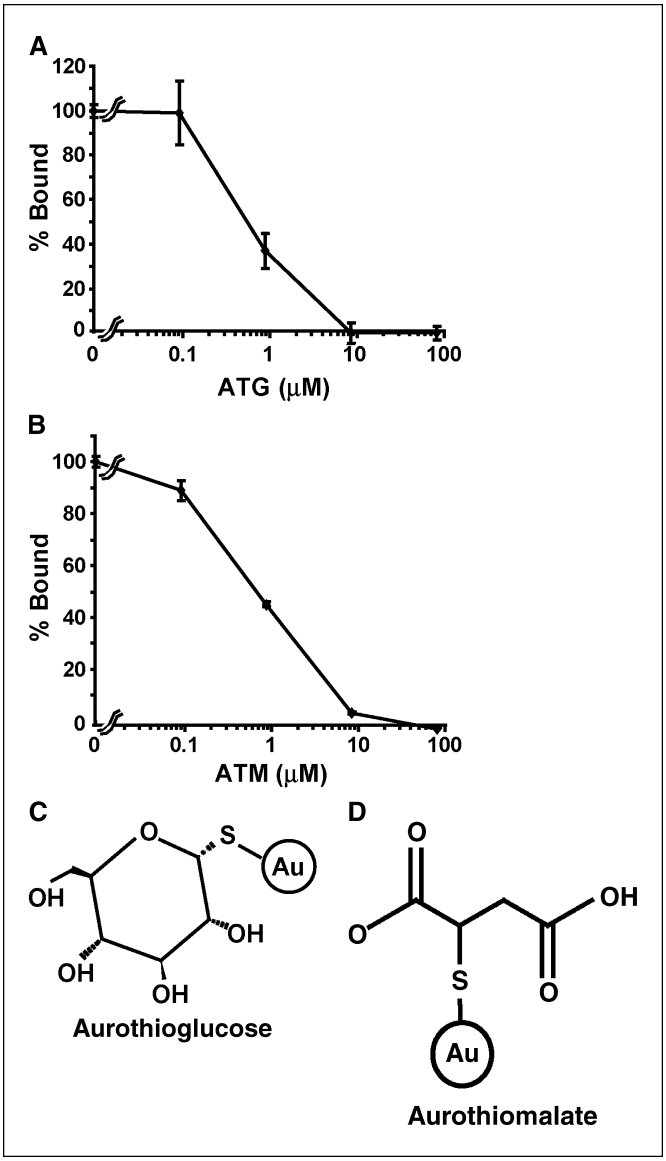

Figure 4. ATG and the related gold compound ATM inhibit binding of PKCι/YFP to Par6. *A* and *B,* biotinylated Par6 was bound to streptavidin-coated plates and incubated with 4,000 relative fluorescence units of PKCι/YFP in the presence of ATG or the closely related gold compound ATM at the indicated concentrations. *Points,* mean (n = 3); *bars,* SE. *C* and *D,* chemical structures of ATG and ATM, respectively.

determined by quantifying the amount of PKCι/YFP fluorescence bound to the plates in the presence of increasing concentrations of ATG (Fig. 4*A*). As can be seen, addition of increasing concentrations of ATG to the binding mixture led to a dose-dependent loss of bound PKCι/YFP. In this assay, maximal inhibition of binding was achieved at 10 μmol/L ATG with an apparent IC_{50} of ~1 μmol/L, in line with the values obtained in our initial FRET-based screen. In addition to ATG, we also tested ATM, a structurally related gold-containing compound that is also used in the treatment of rheumatoid arthritis. Like ATG, ATM caused a dose-dependent loss of PKCι/YFP binding with potency similar to ATG (Fig. 4*B*). Taken together, these results provide confirmation of our initial drug screen and show that both ATG and ATM are potent inhibitors of PKCι-Par6 interactions *in vitro* with apparent IC_{50}s in the low micromolar range. Examination of the chemical structures of ATG

and ATM reveals that a similar thio gold moiety is likely to be involved in their inhibitory activity (Fig. 4*C* and *D*).

ATG inhibits PKCι-mediated cellular signaling. Having identified ATG as an inhibitor of binding between Par6 and PKCι, we next assessed whether ATG was an effective inhibitor of PKCι signaling in cells. We recently showed that PKCι plays a requisite role in the transformed growth of human lung adenocarcinoma A549 cells through activation of the small molecular weight GTPase Rac1 (3). Expression of a dominant-negative kdPKCι leads to inhibition of Rac1 activation and transformed growth of A549 cells (3). The PKCι-dependent activation of Rac1 involves the PB1 domain of PKCι because expression of the PB1 domain of PKCι inhibits coupling of PKCι to Rac1 activation. Others have shown that Par6 couples PKCι to Rac1 by binding PKCι via its PB1 domain while also binding Rac1 through a distinct CRIB domain (Fig. 5*A*; for a review, see ref. 13). Thus, we hypothesized that if ATG disrupts binding between PKCι and Par6, it should block PKCι-mediated activation of Rac1. Indeed, incubation of A549 cells with increasing concentrations of ATG leads to a dose-dependent decrease in Rac1 activity (Fig. 5*B*). At 10 and 100 μmol/L ATG, inhibition of Rac1 activity was comparable to that observed in A549 cells expressing kdPKCι, which we previously showed disrupts PKCι-dependent Rac1 activation (3, 9). Quantitative analysis of multiple independent experiments showed that 10 μmol/L ATG is equipotent with kdPKCι at inhibiting Rac1 activity (Fig. 5*C*). ATG at 100 μmol/L had no further inhibitory effect on Rac1 (data not shown). It should be noted that not all Rac1 activity is PKCι dependent, a finding that is not surprising, considering the many potential upstream effectors of Rac1 activity. These data are consistent with the apparent IC_{50} of ATG for inhibition of the Par6-PKCι interaction *in vitro* because on a pharmacologic basis, one would expect a concentration of drug 10-fold higher than the IC_{50} to cause near complete inhibition. Similar results were obtained with ATM, confirming the ability of a structurally related compound to inhibit PKCι signaling (data not shown).

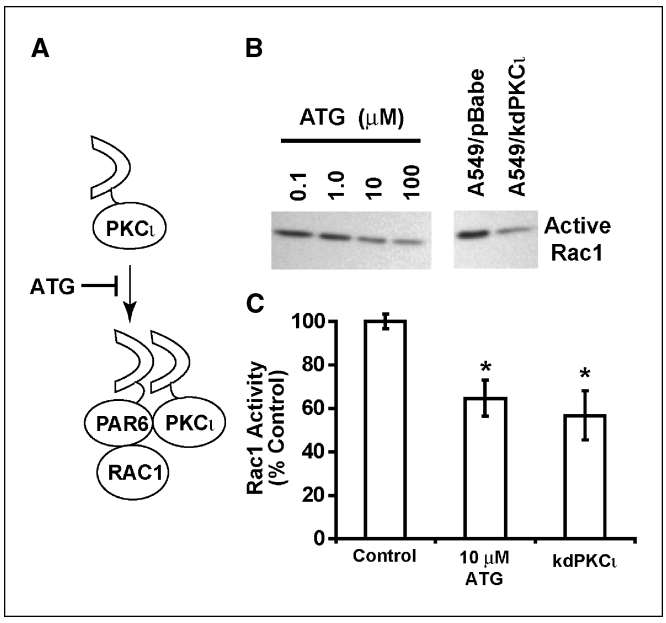

Figure 5. ATG inhibits PKCι-dependent activation of Rac1. *A,* schematic diagram illustrating how Par6 mediates coupling between PKCι and Rac1 by binding these proteins via distinct binding domains on Par6. *B,* A549 cells were treated with ATG at the concentrations indicated and assayed for active, GTP-bound Rac1 as previously described (3). Expression of kdPKCι in A549 cells also leads to Rac1 inhibition. *C,* active and total Rac1 was assessed in A549 cells treated with 10 μmol/L ATG and in cells transfected with kdPKCι. Rac1 activity is expressed as active, GTP-bound Rac1/total Rac1. *Columns,* mean (n = 3); *bars,* SE; *, $P < 0.05$, compared with control cells.

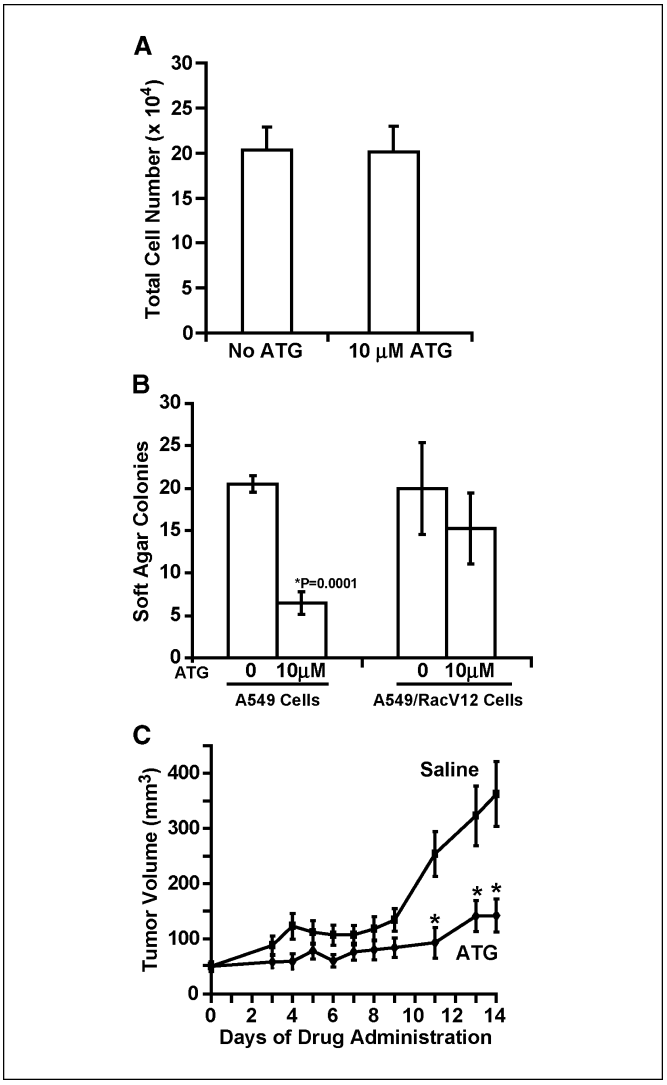

Figure 6. ATG inhibits the transformed growth of A549 cells *in vitro* and *in vivo*. *A,* anchorage-dependent growth of A549 cells in the presence or absence of 10 μmol/L ATG. *Columns,* mean (n = 3); *bars,* SE. *B,* anchorage-independent growth of A549/LZRS and A549/RacV12 cell transfectants in soft agar in the presence or absence of 10 μmol/L ATG. *Columns,* mean (n = 4); *bars,* SE. *, $P = 0.0001$, compared with cells treated with diluent (0.1% DMSO). *C,* tumorigenic growth of A549 cells as s.c. xenografts in nude mice. Mice were injected daily with ATG (200 mg/kg) or vehicle for 14 days and tumor volume was monitored as previously described (3). *Points,* mean (n = 10); *bars,* SE. *, $P < 0.05$.

ATG blocks PKCι-dependent transformation and tumorigenicity. We recently showed that expression of kdPKCι has no effect on A549 cell survival or growth in adherent culture but has a dramatic inhibitory effect on transformed growth *in vitro* and *in vivo* (3). Therefore, we assessed whether the effects of ATG on adherent versus transformed growth of A549 cells were similar to kdPKCι. Addition of 10 μmol/L ATG to adherent cultures of A549 cells had no appreciable effect on cell growth (Fig. 6*A*) or survival (data not shown), consistent with the effect of kdPKCι under adherent growth conditions (3). However, 10 μmol/L ATG resulted

in a significant reduction in the ability of A549 cells to grow as colonies in soft agar (Fig. 6*B*). These results are entirely consistent with our results using kdPKCι (3).

We previously showed that expression of a constitutively active Rac1 mutant, RacV12, in cells expressing kdPKCι restores their transformed growth in soft agar (3, 9). If, as our data indicate, ATG disrupts the PKCι-Par6 complex, thereby inhibiting PKCι-dependent activation of Rac1, then expression of RacV12 should cause cells to be resistant to the inhibitory effects of ATG. Indeed, A549/RacV12 cells grow as soft agar colonies equally well in the absence and presence of 10 μmol/L ATG (Fig. 6*B*). These results provide genetic evidence for a mechanism of action of ATG as an inhibitor of PKCι signaling upstream of Rac1.

We next assessed whether ATG is an effective therapeutic agent against A549 cell tumor growth *in vivo*. Athymic nude mice were injected with A549 cells to establish s.c. tumors. Once tumors were established, the mice were randomly divided into two groups that received daily injections of either ATG (200 mg/kg) or diluent (0.9% saline), and tumor volume was monitored as previously described (3). In the presence of ATG, A549 cell tumors exhibited a dramatic reduction in growth kinetics compared with control tumors (Fig. 6*C*). Our results indicate that ATG has a cytostatic rather than cytotoxic effect on A549 tumors. A similar cytostatic effect was observed in A549 cell tumors expressing kdPKCι (3), consistent with a mechanism of action for ATG at the level of inhibition of PKCι signaling.

Discussion

We recently showed that the atypical PKC isozyme PKCι is an oncogene in NSCLC (4). Specifically, we showed that PKCι expression is elevated in the vast majority of NSCLC cases and that PKCι expression is predictive of poor clinical outcome (4). We also showed that the PKCι gene undergoes frequent tumor-specific genetic alteration by gene amplification in NSCLC. PKCι gene amplification drives PKCι expression, showing the functional importance of gene amplification in NSCLC tumorigenesis (4). Mechanistically, we showed that PKCι plays a requisite role in transformed growth by activating a PKCι→Rac1→Pak→Mek→Erk signaling axis that drives transformed growth (3). Our data indicated that PKCι signaling is an attractive target for development of novel mechanism-based therapeutics for the treatment of lung cancer.

In an effort to develop therapeutics targeting PKCι, we developed a novel high-throughput assay to screen for compounds that inhibit PKCι signaling. Our FRET assay is based on our previous observation that PKCι-dependent transformation requires the PB1 domain of PKCι and coupling of PKCι to the downstream effector Rac1 (3). There is ample evidence that PB1-PB1 domain interactions between PKCι and the adapter molecule Par6 are responsible for coupling PKCι to Rac1 during the establishment of epithelial cell polarity (14). Based on these observations, we reasoned that PB1-PB1 domain interactions between Par6 and PKCι represent a viable drug target for the development of antitumor agents. Through a high-throughput screen of a compound library consisting of 960 drugs that have been used in humans, we identified a promising antitumor agent, ATG. ATG and the related gold compound ATM have been used for many years in the treatment of rheumatoid arthritis (15). However, their use has become limited recently due to the development of effective nonsteroidal anti-inflammatory drugs with efficacy against rheumatoid arthritis and lower toxicity. Despite their extensive use in clinical practice, the precise mechanism of action of gold compounds in rheumatoid arthritis is largely unknown. These compounds exhibit potent anti-inflammatory properties that have been postulated to be mediated through inhibition of nuclear factor κB (NF-κB) signaling (16, 17). However, the molecular mechanism underlying the ability of these compounds to inhibit NF-κB signaling has not been definitively elucidated although a recent report indicated that gold compounds may inhibit NF-κB signaling through inhibition of IκB kinase activation (18).

In the present study, we identified ATG (and ATM) as potent inhibitors of PB1 domain–mediated interactions between Par6 and PKCι. Both ATG and ATM inhibit this interaction in a dose-dependent manner with an apparent IC_{50} in the low micromolar range. Biochemical evidence for this mechanism of action in intact cells is provided by our observation that ATG blocks PKCι-mediated activation of the downstream effector of the Par6-PKCι interaction, Rac1. Indeed, 10 μmol/L ATG causes complete inhibition of PKCι-dependent Rac1 activation, consistent with the fact that this concentration of ATG also elicits maximal inhibition of Par6-PKCι interactions *in vitro*. Furthermore, expression of a constitutively active Rac1 mutant renders A549 cells resistant to the inhibitory effects of ATG on transformed growth, consistent with a mechanism at the level of PKCι upstream of Rac1.

Interestingly, PB1 domain interactions involving PKCι have also been implicated in the coupling of PKCι to NF-κB signaling in some cell systems (19, 20). In fibroblasts, PKCι has been reported to couple to the NF-κB signalosome through PB1-PB1 domain interactions between PKCι and the adaptor molecule p62 (19, 20). Crystallographic and solution structural analysis of PB1 domain interactions between PKCι and Par6 on the one hand, and between PKCι and p62 on the other hand, indicate that the same binding surface of PKCι mediates binding to both of these two proteins (21–24). These results suggest that ATG is likely to also be a potent inhibitor of PKCι-p62 interactions. If this were the case, one would predict that ATG might inhibit PKCι-dependent activation of NF-κB in cell types in which PKCι couples to NF-κB through p62 interactions. This hypothesis would provide a unifying molecular mechanism underlying the actions of ATG as an anti-inflammatory agent in rheumatoid arthritis and as an antitumor agent in cancer cells. In this regard, we have shown that in A549 cells, PKCι does not effectively couple to NF-κB and that NF-κB is not a critical mediator of oncogenic PKCι signaling (3). We have observed that ATG does not affect NF-κB signaling in A549 cells,[1] consistent with the fact that NF-κB signaling in A549 cells is largely independent of PKCι (3). In future studies, it will be of interest to determine whether ATG inhibits NF-κB in cell systems in which PKCι is tightly coupled to this signaling pathway.

Our present data show that ATG and ATM possess potent antitumor activities against NSCLC *in vitro* and *in vivo*. Our data are consistent with the interpretation that the antitumor effects of ATG and ATM are due to their inhibitory effects on PKCι-Par6 interactions and subsequent coupling to Rac1. Furthermore, the inhibitory actions of ATG are strikingly similar to those obtained when PKCι signaling is genetically disrupted using a dominant-negative PKCι mutant allele, kdPKCι. The potency of ATG as an antitumor agent and as an inhibitor of PKCι-mediated activation of

[1] Unpublished observation.

Rac1 are virtually identical, and reconstitution of Rac1 activity by expression of a constitutively active Rac1 allele, RacV12, provides further genetic evidence for the molecular mechanism of action of ATG revealed here. Our results show that ATG and ATM will be useful in the molecular dissection of PKCι-mediated cellular signaling by providing a pharmacologic mechanism for inhibiting PKCι that is complementary to existing genetic approaches. ATG and ATM also hold promise as potential novel therapeutic agents for the treatment of NSCLC patients. With regard to the potential clinical use of ATG and/or ATM as antitumor agents, it is important to note that in our studies, we achieved maximal inhibition of PKCι signaling in NSCLC at concentrations of 10 μmol/L. Pharmacokinetic studies on rheumatoid arthritis patients receiving a standard regimen of gold therapy with ATG or ATM show that steady-state blood levels in the 10 μmol/L range are routinely achievable with limited adverse toxicity (25). Thus, it is likely that therapeutically relevant levels of ATG can be achieved in cancer patients using well-established dosing regimens already approved for rheumatoid arthritis. Further preclinical studies will be required to evaluate the efficacy of ATG and ATM as single agents in multiple preclinical NSCLC tumor models and to assess whether ATG and/or ATM might be effective in combination with existing standards of therapy for NSCLC. It will also be of interest to assess whether these agents also show efficacy against other tumor types. In conclusion, our present results show the utility of targeting protein-protein interactions involving PKCι in the development of novel therapeutics with promise as antitumor agents. In addition, the currently available aurothiogold compounds ATG and ATM should be considered as promising candidates for clinical trials in the treatment of NSCLC.

Acknowledgments

Received 9/22/2005; revised 11/21/2005; accepted 11/23/2005.

Grant support: Mayo Foundation.

The costs of publication of this article were defrayed in part by the payment of page charges. This article must therefore be hereby marked *advertisement* in accordance with 18 U.S.C. Section 1734 solely to indicate this fact.

We thank Dr. D. Zacharias for expert advice on the design and implementation of FRET-based assays and Dr. Chris Eckman (Department of Neuroscience, Mayo Clinic, Jacksonville, FL) for providing the Microsource GenPlus chemical library and for advice on high-throughput drug screening.

References

1. American Cancer Society. Surveillance research cancer statistics. Atlanta: American Cancer Society; 2004.
2. Schiller JH. Current standards of care in small-cell and non-small-cell lung cancer. Oncology 2001;61 Suppl 1:3–13.
3. Regala RP, Weems C, Jamieson L, Copland JA, Thompson EA, Fields AP. Atypical protein kinase Cι plays a critical role in human lung cancer cell growth and tumorigenicity. J Biol Chem 2005;280:31109–15.
4. Regala RP, Weems C, Jamieson L, et al. Atypical protein kinase Cι is an oncogene in non-small cell lung cancer. Cancer Res 2005;65:8905–11.
5. Murray NR, Fields AP. Atypical protein kinase Cι protects human leukemia cells against drug-induced apoptosis. J Biol Chem 1997;272:27521–4.
6. Miyawaki A, Tsien RY. Monitoring protein conformations and interactions by fluorescence resonance energy transfer between mutants of green fluorescent protein. Methods Enzymol 2000;327:472–500.
7. Tsien RY. The green fluorescent protein. Annu Rev Biochem 1998;67:509–44.
8. Murray NR, Jamieson L, Yu W, et al. Protein kinase Cι is required for ras transformation and colon carcinogenesis *in vivo*. J Cell Biol 2004;164:797–802.
9. Zhang J, Anastasiadis PZ, Liu Y, Thompson EA, Fields AP. Protein kinase C βII induces cell invasion through a Ras/MEK-, PKCι/Rac1-dependent signaling pathway. J Biol Chem 2004;279:22118–23.
10. Moscat J, Diaz-Meco MT. The atypical protein kinase Cs. Functional specificity mediated by specific protein adapters. EMBO Rep 2000;1:399–403.
11. Miyawaki A, Llopis J, Heim R, et al. Fluorescent indicators for Ca^{2+} based on green fluorescent proteins and calmodulin. Nature 1997;388:882–7.
12. Pollok BA, Heim R. Using GFP in FRET-based applications. Trends Cell Biol 1999;9:57–60.
13. Suzuki A, Yamanaka T, Hirose T, et al. Atypical protein kinase C is involved in the evolutionarily conserved par protein complex and plays a critical role in establishing epithelia-specific junctional structures. J Cell Biol 2001;152:1183–96.
14. Etienne-Manneville S, Hall A. Cell polarity: Par6, aPKC and cytoskeletal crosstalk. Curr Opin Cell Biol 2003;15:67–72.
15. Messori L, Marcon G. Gold complexes in the treatment of rheumatoid arthritis. Met Ions Biol Syst 2004;41:279–304.
16. Bratt J, Belcher J, Vercellotti GM, Palmblad J. Effects of anti-rheumatic gold salts on NF-κB mobilization and tumour necrosis factor-α (TNF-α)-induced neutrophil-dependent cytotoxicity for human endothelial cells. Clin Exp Immunol 2000;120:79–84.
17. Yamashita M, Ashino S, Oshima Y, Kawamura S, Ohuchi K, Takayanagi M. Inhibition of TPA-induced NF-κB nuclear translocation and production of NO and PGE2 by the anti-rheumatic gold compounds. J Pharm Pharmacol 2003;55:245–51.
18. Jeon KI, Jeong JY, Jue DM. Thiol-reactive metal compounds inhibit NF-κB activation by blocking IκB kinase. J Immunol 2000;164:5981–9.
19. Sanz L, Diaz-Meco MT, Nakano H, Moscat J. The atypical PKC-interacting protein p62 channels NF-κB activation by the IL-1-TRAF6 pathway. EMBO J 2000;19:1576–86.
20. San L, Sanchez P, Lallena MJ, Diaz-Meco MT, Moscat J. The interaction of p62 with RIP links the atypical PKCs to NF-κB activation. EMBO J 1999;18:3044–53.
21. Lamark T, Perander M, Outzen H, et al. Interaction codes within the family of mammalian Phox and Bem1p domain-containing proteins. J Biol Chem 2003;278:34568–81.
22. Hirano Y, Yoshinaga S, Ogura K, et al. Solution structure of atypical protein kinase C PB1 domain and its mode of interaction with ZIP/p62 and MEK5. J Biol Chem 2004;279:31883–90.
23. Hirano Y, Yoshinaga S, Takeya R, et al. Structure of a cell polarity regulator, a complex between atypical PKC and Par6 PB1 domains. J Biol Chem 2005;280:9653–61.
24. Wilson MI, Gill DJ, Perisic O, Quinn MT, Williams RL. PB1 domain-mediated heterodimerization in NADPH oxidase and signaling complexes of atypical protein kinase C with Par6 and p62. Mol Cell 2003;12:39–50.
25. Blocka KL, Paulus HE, Furst DE. Clinical pharmacokinetics of oral and injectable gold compounds. Clin Pharmacokinet 1986;11:133–43.